Structural insights into a HECT-type E3 ligase AREL1 and its ubiquitination activities *in vitro*

Received for publication, July 26, 2019, and in revised form, November 7, 2019 Published, Papers in Press, November 15, 2019, DOI 10.1074/jbc.RA119.010327

Sunil Singh[1], **Joel Ng**, **Digant Nayak**, and **J. Sivaraman**[2]

From the Department of Biological Sciences, 14 Science Drive 4, National University of Singapore, 117543 Singapore

Edited by George N. DeMartino

The HECT E3 ligase family comprises three subfamilies: NEDD4 E3 ubiquitin protein ligase (NEDD4), HECT and RLD domain–containing E3 ubiquitin protein ligase (HERC), and "other." Most previous studies have focused on the NEDD4 subfamily. Apoptosis-resistant E3 ligase 1 (AREL1) belongs to "other" subfamily HECT that inhibits apoptosis by ubiquitinating and degrading proapoptotic proteins. Here, we report the crystal structure of the extended HECT domain of AREL1 (amino acids (aa) 436–823) at 2.4 Å resolution and its ubiquitination of the proapoptotic protein second mitochondria-derived activator of caspase (SMAC). We found that the extended HECT domain adopts an inverted, T-shaped, bilobed conformation and harbors an additional loop (aa 567–573) absent in all other HECT members. We also show that the N-terminal extended region (aa 436–482) preceding the HECT domain is indispensable for its stability and activity and that without this region, the HECT domain becomes inactive. AREL1 ubiquitinated SMAC, primarily on Lys^{62} and Lys^{191}. We solved the crystal structure of the tetrameric form of SMAC to 2.8 Å resolution, revealing the Lys^{62} and Lys^{191} locations. The AREL1 HECT domain assembled Lys^{33}-, Lys^{48}-, and Lys^{63}-linked polyubiquitin chains. Moreover, E701A substitution in the AREL1 HECT domain substantially increased its autopolyubiquitination and SMAC ubiquitination activity, whereas deletion of the last three amino acids at the C terminus completely abrogated AREL1 autoubiquitination and reduced SMAC ubiquitination. Finally, an AREL1-specific ubiquitin variant inhibited SMAC ubiquitination *in vitro*. Our findings may assist in the development of AREL1 inhibitors that block its anti-apoptotic activity in cancer.

The ubiquitin-linked post-translational modification of proteins affects various cellular processes, including protein degradation (1), intracellular trafficking (2), inflammatory response (3), antigen presentation, and post-replicational DNA repair (4). The ubiquitination process involves the enzymatic activities of E1 (ubiquitin-activating), E2 (ubiquitin-conjugating), and E3 (ubiquitin ligase) enzymes (5). E3 ubiquitin ligases provide specificity to the reaction, by bringing together the E2-ubiquitin thioester and the substrate to catalyze isopeptide bond formation during the ubiquitination process. E3 ligases are grouped into three different classes: RING[3] (really interesting new gene); HECT (homologous to the E6-AP C terminus), and RBR (RING between RING) types. Members of the RING and RBR E3 ligases are well-characterized and are key regulators of numerous cellular signaling pathways (6). In contrast, HECT E3 ligases are less well-characterized.

HECT-type E3 ligases have a conserved ~40-kDa C-terminal HECT domain, which displays 16–92% amino acid identity across its 28 members in humans. Dysfunction of these HECT-type E3 ligases is associated with the genesis of several human diseases, including cancer, autoimmunity, hypertension, and neurological disorders (7). HECT-type E3 ligases perform a two-step ubiquitination process, in which the catalytic cysteine residue in the HECT domain accepts ubiquitin from the E2-Ub thioester intermediate and subsequently mediates the transfer of this ubiquitin moiety to the lysine residue on the substrate protein to form an isopeptide bond. The nature of the polyubiquitin chain linkage type that occurs on the substrate determines its fate (8) and is generally dictated by E2 enzymes. However, HECT-type E3 ligases have the ability to assemble specific ubiquitin chain linkages on substrates, which is independent of E2-specific ubiquitin assembly (9).

HECT-type E3 ligases are subgrouped into three subfamilies based on various N-terminal substrate-binding domains. Among the 28 HECT-type E3s, nine belong to the NEDD4 subfamily, members of which comprise an N-terminal C2 domain and 2–3 WW domains. The NEDD4 subfamily of HECT-type E3s is structurally and functionally well-characterized, with evidence that NEDD4-type E3s predominantly assemble Lys^{63}-polyubiquitin linkages (10). Structural analysis of NEDD4 HECT domain shows that it forms a bilobed structure consisting of a large N-lobe and a small C-lobe (9). The HERC-type E3 ligase subfamily consists of six members, each bearing the regulator of chromatin condensation 1 (RCC-1)-like domain

This work was supported in part by Ministry of Education, Singapore, Grants R-154-000-B03-112 (MoE Tier 2) and R154-000-A72-114 (AcRF Tier 1). The authors declare that they have no conflicts of interest with the contents of this article.

This article contains Tables S1–S5 and Figs. S1–S10.

The atomic coordinates and structure factors (codes 6JX5 and 6JX6) have been deposited in the Protein Data Bank (http://wwpdb.org/).

The mass spectrometry proteomics data have been deposited in the ProteomeXchange Consortium via the PRIDE partner repository with the data set identifier PXD016016.

[1] Graduate scholar in receipt of a research scholarship from NUS.

[2] To whom correspondence should be addressed. E-mail: dbsjayar@nus.edu.sg.

[3] The abbreviations used are: RING, really interesting new gene; HECT, homologous to the E6-AP C terminus; RBR, RING between RING; AREL1, apoptosis-resistant E3 ligase 1; aa, amino acid(s); IAP, inhibitor of apoptosis; r.m.s., root mean square; PDB, Protein Data Bank; Ub, ubiquitin; UbV, Ub variant; GST, glutathione *S*-transferase; SMAC, second mitochondria-derived activator of caspase.

(RLD). The remaining 13 HECT members have no uniformity and comprise the "other" subfamily of HECT-type E3 ligases. Members of this "other" subfamily control virtually every major cellular process in eukaryotes (11–13). Despite this, there is a limited understanding of the overall ubiquitination mechanism of this subfamily. A better understanding of the structural and functional roles of these E3 ligases would greatly assist in the development of therapeutic selective inhibitors or modulators for a range of diseases and disorders.

AREL1 (apoptosis-resistant E3 ligase 1) is an 823-aa anti-apoptotic HECT-type E3 ubiquitin ligase assigned to the "other" subfamily. The HECT domain of AREL1 shows a 35% sequence identity with the HECT domain of members from the NEDD4 subfamily and between 20 and 33% identity with "other" subfamily members; this highlights the diversity of this HECT subfamily. Studies have shown that AREL1 overexpression confers apoptotic resistance in H1299 cells, but its knockdown leads to increased sensitivity to apoptosis (13).

Apoptosis is a physiological cell death process regulated by three main factors: the inhibitor of apoptosis (IAP) family of proteins; the IAP antagonists, such as SMAC, HtrA2, and ARTS proteins; and the caspases (14). The IAP family functions to block cell death by regulating the activity of initiator and effector caspases via their conserved BIR domains, which can bind to caspases (15). The IAP family is, in turn, regulated by a class of inhibitor proteins known as IAP antagonists, which induce apoptosis through both caspase-dependent and -independent mechanisms (16). A previous study has shown that AREL1 mediates the degradation of SMAC, HtrA2, and ARTS, conferring apoptotic resistance to a range of cancer cells (13). Notably, AREL1 assembles atypical Lys^{33}-linked polyubiquitin chains (17, 18); however, the biological significance of such chains is less explored, and there is no structural understanding of how HECT E3s are involved in such atypical chain synthesis.

As a continuation of our studies on elucidating the mechanisms of E3 ligases (19–23), here we report the structure of an extended HECT domain of AREL1 (aa 436–823), containing an additional N-terminal region preceding the HECT domain. This additional N-terminal region (aa 436–482) is indispensable for the activity and stability of the domain, and the N-lobe and C-lobe in the extended AREL1 HECT domain are arranged in an inverted T-shaped conformation. Notably, the extended AREL1 HECT domain contains an additional loop (aa 567–573), which is absent in all other HECT members. We show that a point mutation (E701A) in the AREL1 HECT domain increases its autopolyubiquitination and substrate ubiquitination activity. Moreover, we demonstrate that an AREL1-specific ubiquitin variant can regulate AREL1-mediated SMAC ubiquitination. The potential oncogenic role of AREL1 parallels with studies of other characterized HECT E3s, and our study enhances the understanding of the structural and functional diversity of the "other" subfamily of HECT E3 ligases.

Results

Structure of the extended AREL1 HECT domain

A sequence comparison of AREL1 with other HECT E3 ligases was used to predict the importance of the N-terminal extended region (~50 aa; aa 436–482, including an α1 helix) preceding the HECT domain (Fig. S1). We generated two AREL1 constructs— one with (aa 436–823) and one without (aa 483–823) the extended region—to test the significance of the extended region (Fig. 1*A*). We observed that the AREL1 construct without the extended region was unstable and less soluble, whereas the AREL1 construct with the extended region was soluble. However, crystallization experiments with the extended AREL1 HECT construct (aa 436–823) could not be performed, as the protein precipitated during the concentration step and could not reach a sufficiently high concentration (~10–12 mg/ml) for crystallization trials. As one of our approaches toward improving protein quality for crystallization, we performed reductive alkylation of the protein sample following gel filtration chromatography (24). This modification significantly improved protein quality and led to the formation of crystals. These crystals diffracted up to 2.4 Å, and the structure was determined (Table 1). The asymmetric unit contains three molecules of extended AREL1 HECT domain (Fig. S2).

HECT domains adopt two different conformations, an inverted T-shape and an open L-shape, based on the movement of the C-lobe around the flexible hinge region (25). Here, we observed that the extended AREL1 HECT domain adopts an inverted T-shape and forms a canonical bilobed structure of an N-lobe and a C-lobe (Fig. 1*B*). The N-lobe consists of two subdomains, a large subdomain (aa 483–589 and 669–705) and a small subdomain (aa 595–668), which are connected through a short linker (aa 590–594) (Fig. 1*B*). The residues in the extended region (aa 436–482) shield the hydrophobic surface on the N-lobe large subdomain, which stabilizes AREL1. The N-lobe large subdomain contains 11 α-helices (α1–α11) and four β-strands (β1–β4). The N-lobe small subdomain—involved in the E2 interaction— comprises three α-helices (α7–α9) and two β-strands (β3 and β4). The N-lobe and C-lobe are also connected via a short, flexible hinge region (aa 706–711) (Fig. 1*B*). The C-lobe (aa 712–823) possesses the catalytic cysteine residue (Cys^{790}) and contains five α helices (α12–α16) and four β strands (β5–β8) (Fig. 1*B*). Notably, the N-lobe large subdomain contains an additional loop (aa 567–573), which is absent in all other HECT E3 family members. This additional loop highlights the diversity within the HECT family.

Close inspection of the N-lobe and C-lobe allowed us to identify the residues involved in the interactions of the inverted T-shape conformation of the AREL1 HECT domain (Table S3). Hydrogen bonds are formed between an N-lobe Glu^{701} and three residues on the C-lobe (Gln^{753}, Ser^{759}, and Gln^{760}) as well as between an N-lobe Asn^{698} and C-lobe Gln^{753} (Fig. 1*C*). Notably, all members of the NEDD4 HECT E3 ligase subfamily contain a conserved N-lobe tyrosine residue that makes a hydrogen bond with a C-lobe threonine residue (26). However, in the AREL1 HECT domain, the tyrosine is replaced by glutamine (Gln^{534}), which forms hydrogen bonds with C-lobe residues Thr^{756} and Asn^{792} (Fig. 1*C*). In addition, N-lobe Arg^{579} and Glu^{599} form hydrogen bonds with C-lobe residues Gln^{760} and Thr^{789}, respectively. The extensive interactions between the N-lobe and C-lobe residues stabilize the inverted T-shape conformation of the HECT domain and position the catalytic cysteine residue near the E2-binding site.

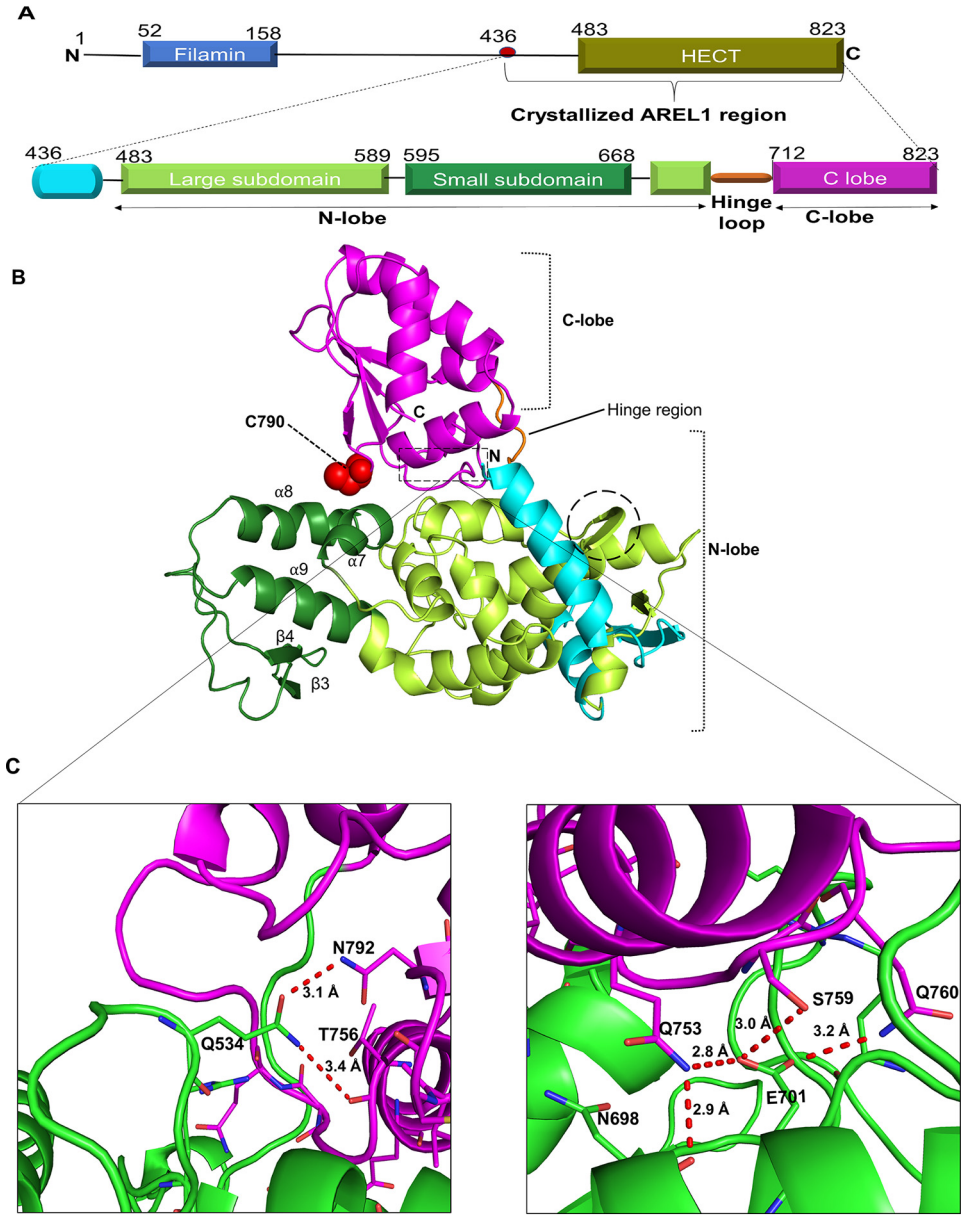

Figure 1. Domain architecture and structure of the extended AREL1 HECT domain. *A*, domain architecture of AREL1 and constructs used in this study. Full-length AREL1 contains the N-terminal filamin domain and C-terminal HECT domain. *B*, crystal structure showing that the extended AREL1 HECT forms an inverted T shape conformation. The N-lobe large subdomain is *colored* in *light green*, and the N-lobe small subdomain is *colored* in *dark green*. The N-lobe small subdomain contains the E2 binding site, and the C-lobe (*colored magenta*) contains the catalytic cysteine (*C790*). The N-terminal extended region (aa 436–482) preceding the HECT domain is *colored cyan*, and the additional loop region in the N-lobe large subdomain is indicated with a *dashed black circle*. *C*, *close view representation* of N-lobe and C-lobe in the extended AREL1 HECT domain. Shown is identification of essential residues involved in extensive hydrogen bond formation. The N-lobe is *colored green*, and the C-lobe is *colored magenta*. All of the interacting residues are shown in *stick representation*. The hydrogen bonds are highlighted as a *red dashed line* and the distances are indicated.

A DALI (27) search using the extended AREL1 HECT domain identified several homologs from the HECT E3 ligase family. These included members of the NEDD4 subfamily; the extended AREL1 HECT domain closely resembles that of WWP1 (r.m.s. deviation: 2.3 Å for 352 Cα atoms). Moreover, there is structural similarity between AREL1 and HUWE1, a member of the "other" subfamily (r.m.s. deviation 2.8 Å for 354 Cα). Structural similarity also exists between the N-lobes of the extended AREL1 HECT domain and NEDD4L HECT E3 (inverted T-shape), the crystal structure of which has been solved in complex with the E2 enzyme (r.m.s. deviation 2.1 Å for 211 Cα atoms).

The crystal structure of the NEDD4L HECT domain in complex with UbcH5B showed that its catalytic cysteine residue is <8 Å away from the active-site cysteine residue (Cys^{86}) of UbcH5B (28). The superimposition of the C-lobe of AREL1 on the equivalent region of the NEDD4L-UbcH5B complex (PDB code 3JVZ) showed that this distance is ~7 Å. The observed inverted T-shape conformation of HECT E3 ligases shows the catalytic cysteine being positioned near to the N-lobe small subdomain. A small rotational movement of the C-lobe around the hinge region is required to bring the catalytic cysteine close to the active-site cysteine of the E2 enzyme to allow the trans-thiolation process (29, 30).

Table 1
Data collection and refinement statistics
Statistics for the highest-resolution shell are shown in parentheses.

Data set	Extended AREL1 HECT	SMAC
Data collection		
Wavelength (Å)	0.9792	0.9791
Resolution range (Å)	48.44–2.40 (2.48–2.40)	47.6–2.80 (2.90–2.80)
Space group	C121	$P2_12_12_1$
a, *b*, *c* (Å)	209.156, 121.057, 80.798	82.19, 85.40, 114.66
α, β, γ (°)	90, 91.49, 90	90, 90, 90
Total no. of reflections	438,820	212,051
Unique reflections	77,372 (7296)	19,688 (1880)
R_{meas}	0.120 (0.479)	0.151 (0.557)
R_{pim}	0.049 (0.235)	0.045 (0.202)
CC1/2	0.993 (0.832)	0.996 (0.906)
Completeness (%)	98.66 (93.60)	96.93 (94.47)
Redundancy	5.7 (3.6)	10.5 (7.1)
I/σ	19.22 (2.57)	22.5 (4.0)
Wilson *B*-factor (Å^2)	36.23	65.57
Refinement		
Resolution range (Å)	48.44–2.40 (2.48–2.40)	47.6–2.80 (2.90–2.80)
Reflections used in refinement	77,372 (7296)	19,688 (1880)
Reflections used for R_{free}	3742 (400)	1014 (99)
R_{work} [a]	0.18 (0.23)	0.21 (0.28)
R_{free} [b]	0.21 (0.30)	0.26 (0.37)
Water molecules	366	
Protein residues	1134	600
r.m.s. deviation, bonds (Å)	0.004	0.005
r.m.s. deviation, angles (°)	0.96	0.96
Ramachandran favored (%)	96.90	96.45
Rotamer outliers (%)	0.20	0.20
Clashscore	2.26	8.35
Average *B*-factor (Å^2)	38.97	63.47
Protein atom (Å^2)	38.83	63.47
Water (Å^2)	42.36	

[a] $R_{work} = \Sigma||F_{obs}| - |F_{calc}||/\Sigma|F_{obs}|$, where F_{calc} and F_{obs} are the calculated and observed structure factor amplitudes, respectively.
[b] R_{free} was calculated as was R_{work}, but using ~5% of data excluded from refinement.

Comparison of the E2-binding region among AREL1 and other HECT E3s

One intriguing aspect of the ubiquitination process is the interaction of the HECT domain with different E2 enzymes. The N-lobe small subdomain (~70-aa region) in the HECT domain is responsible for E2 binding, and this region varies considerably across the various HECT family members in terms of amino acid composition. However, within the NEDD4 subfamily, there is a 50–80% identity in this region, with ~10 amino acid residues identified as being involved in E2 interaction (Fig. S4*A*). In the AREL1 HECT domain, the equivalent region (aa 595–668) forms an N-lobe small subdomain, with only four common residues with that of the NEDD4 subfamily HECT E3s. Structural analysis of the AREL1 E2-interacting region shows that this region contains different structural elements, such as α-helices, β-sheets, and loops, in different orientations (Fig. 2, *A–D*) (29–31). Notably, two "other" subfamily HECT domain structures (E6AP and HUWE1) have been determined, and their E2-binding regions have only 20–35% identity with the AREL1 E2-binding region.

The extended AREL1 HECT domain is catalytically active

Autoubiquitination is often used as a marker of E3 ligase activity, and studies have attributed to this feature to be involved in the regulation of the activity, stability, and downstream signaling functions of E3 ligases (30). We first conducted an *in vitro* ubiquitination assay of the extended AREL1 HECT domain with UBA1 (E1), UbcH7 (E2), ubiquitin (Ub), and ATP. SDS-PAGE and Western blot analysis, using immunoblotting with an anti-Ub antibody, showed higher-molecular weight bands than the AREL1 HECT domain alone (Fig. 3, *A* and *B*), indicative of AREL1 HECT-Ub polymers and autoubiquitination. TripleTOF 5600 MS analysis of these bands identified ~11 lysine residues all involved in autoubiquitination (Fig. S5 and Table S5).

Notably, we have also observed weak autoubiquitination of the extended AREL1 HECT domain in the absence of UbcH7 (E2), as shown by the appearance of a higher-molecular weight band corresponding to monoubiquitinated extended AREL1 HECT (Fig. 3*B*, *lane 2*).

Our structural analysis of the extended AREL1 HECT domain showed that Glu^{701} in the N-lobe forms hydrogen bonds with three residues of the C-lobe (Fig. 1*C*). To assess whether it is involved in ubiquitination, we mutated this Glu^{701} to Ala and performed an autoubiquitination assay. Both SDS-PAGE and Western blot analysis highlighted that mutation of Glu^{701} to Ala significantly increased the autopolyubiquitination activity as compared with the WT AREL1 HECT domain (Fig. 3, *C* and *D*). Therefore, Glu^{701} is a critical residue in the AREL1 HECT domain and can alter autopolyubiquitination activity.

The extended AREL1 HECT domain ubiquitinates the substrate SMAC

Previous reports suggest that AREL1 can interact with its substrates in the absence of its N-terminal filamin domain (aa 52–158) (13). Therefore, we next characterized the activity of the extended AREL1 HECT domain in the presence of its substrate, SMAC, using an *in vitro* ubiquitination assay. Both SDS-PAGE and Western blot analysis reveal that the extended AREL1 HECT domain ubiquitinates SMAC via the conjugation of polyubiquitin chains, as noted by the presence of multiple higher-molecular weight bands corresponding to the sizes of mono- and multiubiquitinated SMAC (Fig. 4, *A* and *B*). Consistent with our observations (see above), we noted that the extended AREL1 HECT domain can ubiquitinate SMAC in the absence of E2, albeit at a lower efficiency (Fig. 4*B*, *lane 2*).

The AREL1 E701A mutant showed enhanced autoubiquitination activity (Fig. 3, *C* and *D*), and we were similarly interested in studying the effects of this mutation on SMAC ubiquitination. As such, we performed SMAC ubiquitination with the E701A mutant and compared its activity with the activity of the WT extended AREL1 HECT domain. Notably, we observed an increase in SMAC ubiquitination by the E701A mutant, which highlights that the mutation of the Glu^{701} residue in the AREL1 HECT domain affects both its autoubiquitination and substrate ubiquitination activity (Fig. 4, *C* and *D*).

AREL1 HECT domain assembles Lys^{33}-, Lys^{48}-, and Lys^{63}-linked polyubiquitin chains

We next analyzed the specificity of the polyubiquitin chain linkages assembled by the extended AREL1 HECT domain in an *in vitro* autoubiquitination assay (Fig. 5*A*). This assay was performed with UBA1 (E1), UbcH7 (E2), extended AREL1 HECT domain (E3), and a panel of eight different Lys-to-Arg Ub mutants (K6, K11, K27, K29, K33, K48, and K63) that each

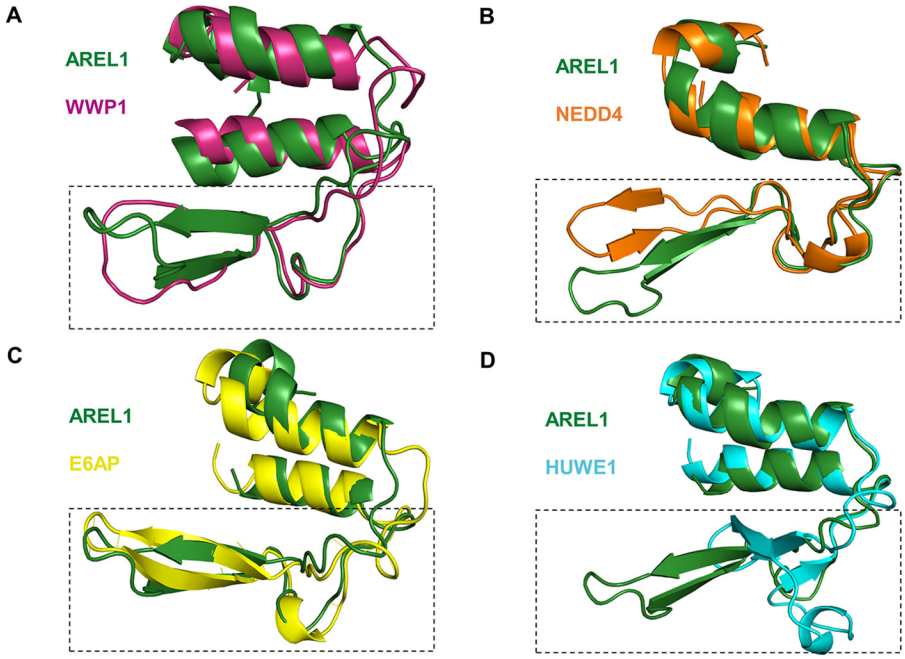

Figure 2. Structural comparison of AREL1 E2 binding region (aa 595- 668) against the E2-binding region of different HECT E3 ligases. Superimposition of E2-binding regions between AREL1 (*dark green*) and WWP1 (*warm pink*) (*A*), NEDD4 (*orange*) (*B*), E6AP (*yellow*) (*C*), and HUWE1 (*cyan*) (*D*). The differences in the secondary structure elements in the E2 binding regions are highlighted by a *dotted rectangular box*.

retained only one lysine residue; K0 has all lysine residues mutated to arginine. Incubation of the extended AREL1 HECT domain with each of the eight different ubiquitination reactions resulted in the formation of mono and di-Ub chains with all mutants, whereas formation of polyubiquitin chains was only observed with K33, K48, and K63 ubiquitin single mutants. The Lys^{33}-, Lys^{48}-, and Lys^{63}-linked chains were significantly longer, and the bands in the Western blotting were of a higher intensity than the other single lysine Ub mutants. The Lys^{48}- and Lys^{63}-linked polyubiquitin chains might allow AREL1 to regulate its activity and stability in the cell; the biological significance of the Lys^{33} linkage remains unknown.

Lys^{61} and Lys^{191} are two major sites on SMAC involved in ubiquitination

Next, we sought to identify the sites on SMAC that are subjected to ubiquitin conjugation by the extended AREL1 HECT domain. Ubiquitinated SMAC bands were analyzed by MS, which identified three lysine residues on SMAC modified with ubiquitin: Lys^{62}, Lys^{191}, and Lys^{207} (Table S5). We performed site-directed mutagenesis to mutate each lysine residue to arginine and generated single (K62R, K191R, and K207R) and double mutants (K62R/K191R, K62R/K207R, and K191R/K207R) (Fig. 5*B*). *In vitro* ubiquitination assays with these single and double mutants highlighted a significant reduction in the ubiquitination of K62R and K191R single mutants and almost no signal in the K62R/K191R double mutant (Fig. 5*B*). There was no significant change in the ubiquitination signal for the K207R mutant. Together, these studies suggest that Lys^{62} and Lys^{191} are the two major sites on SMAC targeted for ubiquitination by AREL1. The Lys^{207} residue might be involved in weak ubiquitination, which could be the reason that no changes were observed in the SMAC ubiquitination when this residue was mutated into arginine. However, in the crystal structure of SMAC (see "Crystal structure of tetrameric SMAC (aa 56–239)"), this residue is not buried in the tetrameric structure.

Crystal structure of tetrameric SMAC (aa 56–239)

To map the positions of Lys^{62} and Lys^{191} on the endogenously relevant tetrameric SMAC structure, we solved the structure of the tetrameric form of SMAC, which is not available in the literature. Previous studies have only captured the monomeric and dimeric forms of SMAC (32, 33). The molecular mass of monomeric SMAC is 20 kDa; however, it naturally exists in an active tetrameric form (~80 kDa) in solution to interact and inhibit IAPs (Fig. S6) (33). Here, we crystallized the tetrameric form of SMAC and determined its structure (Table 1). The final model was refined up to 2.8 Å resolution. There are four molecules in the asymmetric unit (Fig. 5, *C* and *D*). The tetrameric structure of SMAC shows the arrangement of four monomeric chains as a dimer of dimers (chain D and chain A:chain C and chain B). The residues Gln^{116}, Glu^{127}, and Glu^{131} in chain A of one dimer form hydrogen bonds with the Glu^{196}, Gln^{91}, and Gln^{193} residues in chain C of the second dimer, respectively (Fig. S7 and Table S4). The buried surface area between the dimers of the tetramer (*i.e.* between chain A and chain C) is 508.7 $Å^2$ based on the PISA analysis (34).

As discussed in the previous section, AREL1 targets Lys^{62} and Lys^{191} on SMAC for its ubiquitination. Here, we show the arrangement of Lys^{191} on four different monomeric chains of the SMAC tetramer. Lys^{62} could not be mapped in the structure, as it is present at the beginning of the chains, and no electron density was obtained for the initial 16 amino acids.

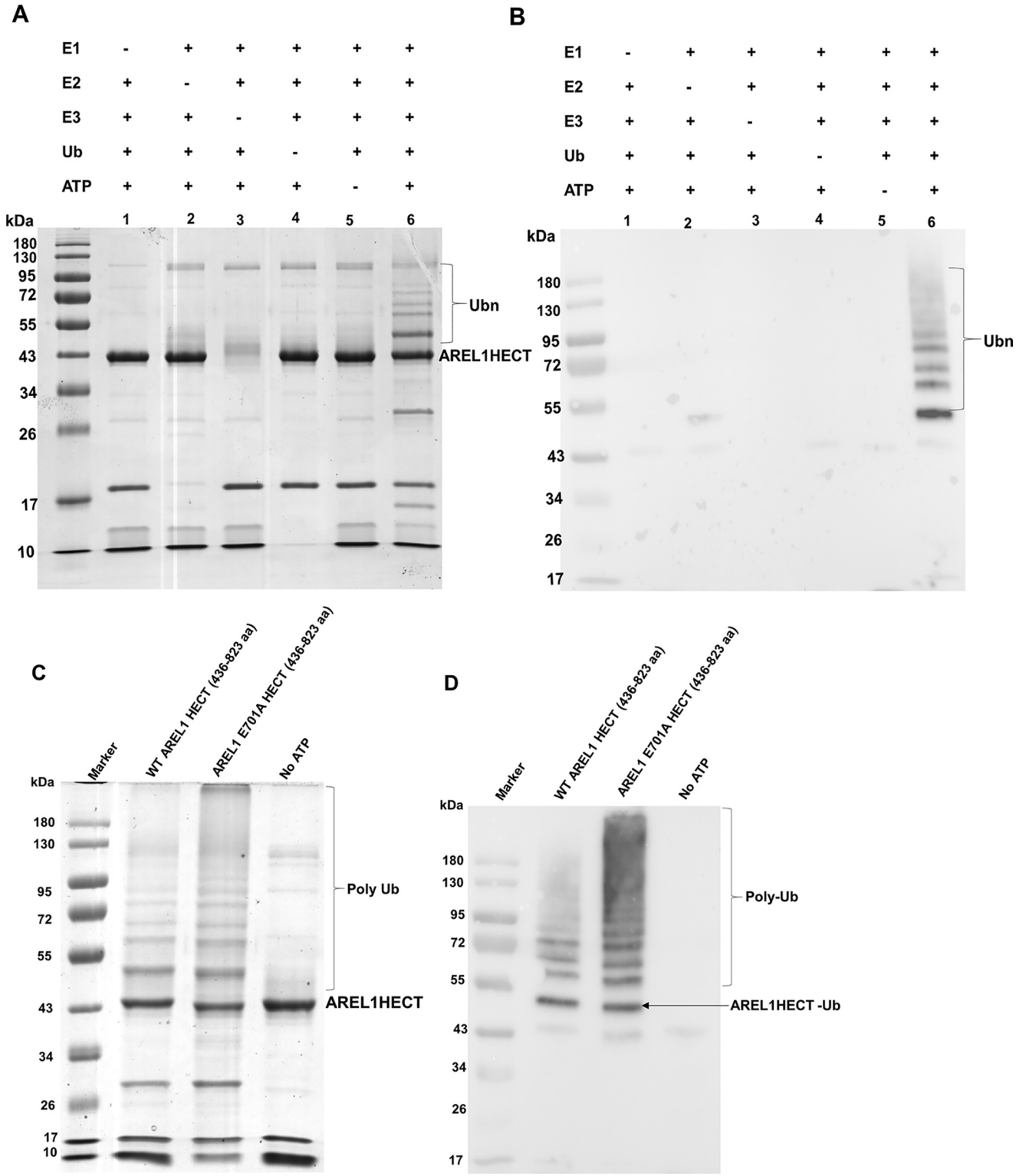

Figure 3. Autoubiquitination activity of the extended AREL1 HECT domain and its E701A mutant. *A*, the various *in vitro* ubiquitination reactions were conducted in the presence (+) or absence (−) of E1 (UBA1), E2 (UbcH7), E3 (extended AREL1 HECT), Ub, and ATP, respectively. SDS-PAGE analysis shows the formation of polyubiquitin chains on the extended AREL1 HECT domain. *B*, Western blot analysis of *A* to highlight the catalytic activity of AREL1 and the activity of AREL1 without E2 enzyme. The AREL1 extended HECT domain autoubiquitination activity can be seen in the absence of E2 enzyme (*lane 2*). The products were immunoblotted with anti-ubiquitin antibody. *C*, SDS-PAGE analysis of *in vitro* ubiquitination reactions to compare the catalytic activities between WT extended AREL1 HECT and its E701A mutant. *D*, Western blot analysis of *in vitro* ubiquitination reactions in *C* to compare the catalytic activities between WT extended AREL1 HECT and E701A mutant. The products were immunoblotted with anti-ubiquitin antibody.

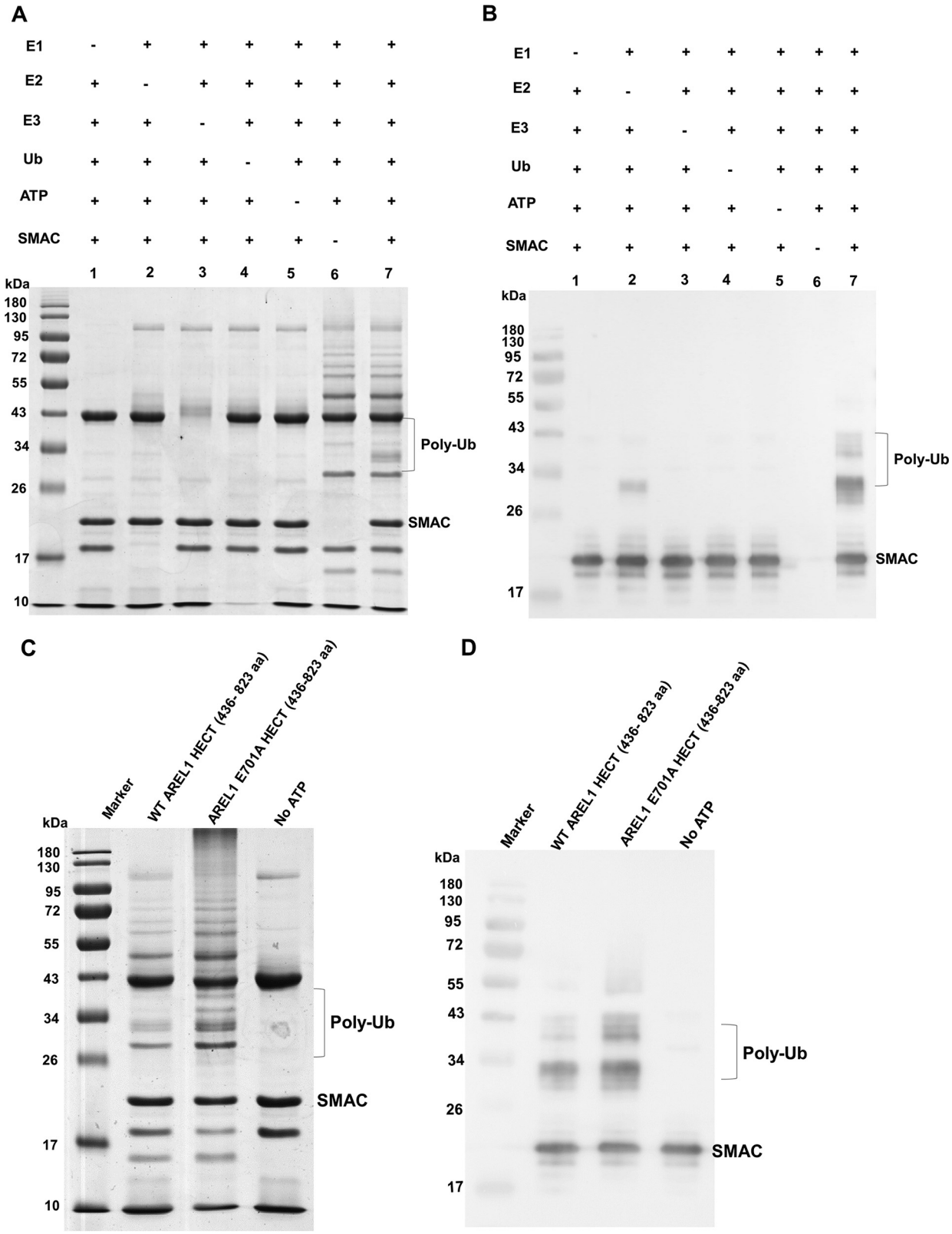

Figure 4. The extended AREL1 HECT ubiquitinates antagonist of inhibitor of apoptosis protein SMAC. *A*, the extended AREL1 HECT domain was incubated in the presence (+) or absence (−) of E1 (UBA1), E2 (UbcH7), WT SMAC, Ub, and ATP in an *in vitro* ubiquitination assay. SDS-PAGE analysis shows that the extended AREL1 HECT domain polyubiquitinates SMAC. The *rightmost lane* (*lane 7*) represents the control lane with all components required for the ubiquitination cascade present. *B*, Western blot analysis of *A* to further highlight AREL1-mediated SMAC ubiquitination. The extended AREL1 HECT domain is functionally active in the absence of E2 (*lane 2*) and ubiquitinates SMAC weakly. The products were immunoblotted with anti-SMAC antibody. *C*, SDS-PAGE analysis to compare the *in vitro* SMAC ubiquitination by WT extended AREL1 HECT domain and its E701A mutant. *D*, Western blot analysis of *in vitro* SMAC ubiquitination by WT extended AREL1 HECT domain and its E701A mutant. The products were immunoblotted with anti-SMAC antibody.

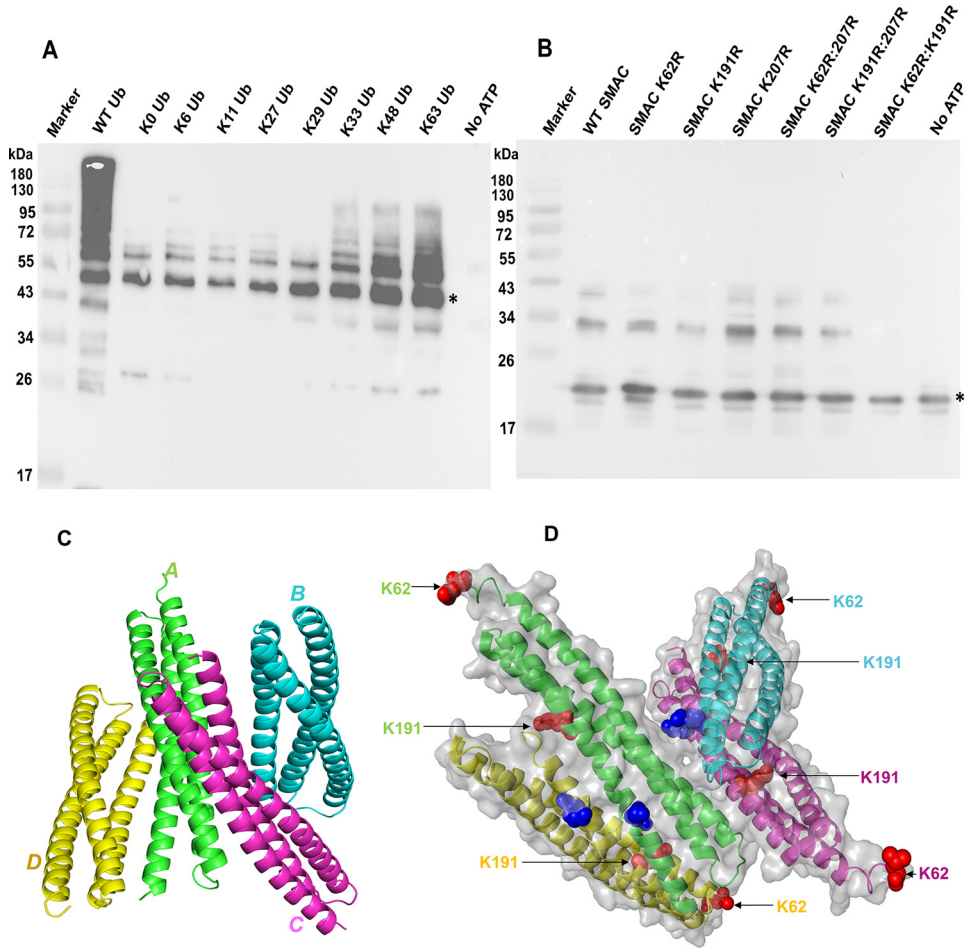

Figure 5. Ubiquitin linkage assembly, sites of ubiquitination on SMAC, and its tetrameric crystal structure. *A*, *in vitro* autoubiquitination assay of the extended AREL1 HECT domain in the presence of WT ubiquitin and single-lysine Ub mutants. Each *lane* represents a Ub mutant with a single lysine residue conserved. A control reaction without ATP was conducted in the *rightmost lane*. The products were blotted with anti-ubiquitin antibodies. *, AREL1-Ub band. *B*, site-directed mutagenesis of SMAC followed by its *in vitro* ubiquitination assay to identify possible ubiquitination sites. The extended AREL1 HECT domain was incubated with E1 (UBA1), E2 (UbcH7), WT SMAC or its mutants, Ub, and ATP in an *in vitro* ubiquitination assay. WT SMAC and its various mutant constructs were used as labeled. The products were blotted with anti-SMAC antibodies. *, SMAC protein band. *C*, crystal structure of the tetrameric form of SMAC showing the arrangement of four SMAC monomers. *D*, Lys^{62} and Lys^{191} ubiquitination sites are highlighted in the SMAC monomers as *red spheres*. The Lys^{207} position is also labeled on the SMAC monomers as *blue spheres*.

Critical role of C-terminal residues of AREL1 HECT domain for ubiquitination

HECT E3s confer ubiquitin chain-type specificity, and it has been shown that the last 60 amino acids of the C-lobe are the determinants of linkage chain specificity (Fig. S4*B*) (35). Members of the NEDD4 subfamily have an invariable acidic residue as the last amino acid, which, if deleted or mutated, can result in WT transthiolation; however, it completely abrogates substrate ubiquitination (10). Notably, HECT E3s in the "other" subfamily do not have this acidic residue, and limited knowledge is available about the involvement of their C-terminal residues in the ubiquitination process. Previous work has shown that deletion of the last amino acid of E6AP ("other" subfamily member whose structure is known) does not affect its ubiquitination activity (36); however, substitution of the last four amino acids of NEDD4 with the last three amino acids of E6AP results in a substantial reduction in chain kinetic formation of the NEDD4 E3 ligase (10). Moreover, a conserved phenylalanine located at the fourth position from the C terminus is critical for HECT E3 substrate ubiquitination (36).

To assess the catalytic role of C-terminal residues of the extended AREL1 HECT domain in autoubiquitination and SMAC ubiquitination, we mutated the Phe residue located at the fourth position from the C terminus of the extended AREL1 HECT domain to alanine (F820A mutant) and generated another mutant without the last three amino acids (Δ3 CT mutant; aa 436–820). Notably, autoubiquitination was undetectable with both F820A and Δ3 CT mutants (Fig. 6, *A* and *B*). For SMAC ubiquitination, no ubiquitination was observed with the F820A mutant, whereas reduced SMAC ubiquitination was observed with the Δ3 CT mutant (Fig. 6, *C* and *D*). The last three amino acids of AREL1 are similar to the last three amino acids of E6AP, and deletion of these amino acids in E6AP did not affect E6AP-mediated p53 multiubiquitination (36). These differences between the AREL1 and E6AP E3 ligases suggest the possibility of differences in catalytic mechanisms.

AREL1-specific Ub variant (UbV), KL.3, modulates AREL1 ubiquitination

A recent screening of selective UbV modulators for different NEDD4 HECT E3s uncovered distinct mechanisms of HECT

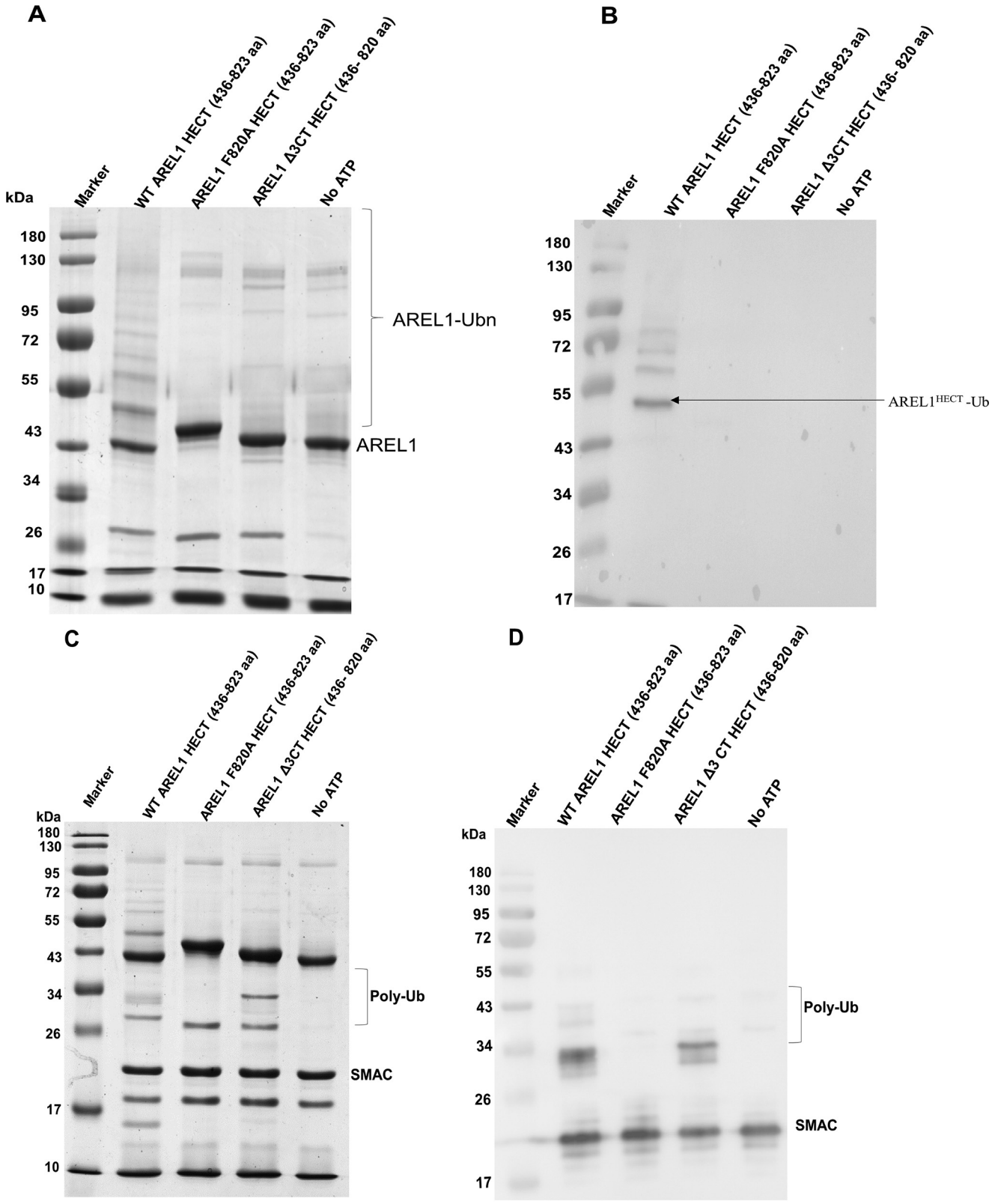

Figure 6. Comprehensive analysis of the role of C-terminal residues of the extended AREL1 HECT domain in autoubiquitination and SMAC ubiquitination. *A*, involvement of C-terminal residues of AREL1 in the ubiquitination process. *In vitro* autoubiquitination assay to compare the catalytic activities of WT AREL1 extended HECT domain with its F820A and Δ3 CT mutants. SDS-PAGE analysis showed complete inhibition of autoubiquitination in both F820A and Δ3 CT mutants. *B*, Western blot analysis of WT extended AREL1 HECT domain and its F820A and Δ3 CT mutants to highlight the role of C-terminal residues on autoubiquitination activity. The products were blotted with anti-Ub antibodies. *C*, SDS-PAGE analysis to show the effects of F820A and Δ3 CT mutations on SMAC ubiquitination as compared with WT AREL1 extended HECT domain. *D*, Western blot analysis to further confirm the role of F820A and Δ3 CT mutations on SMAC ubiquitination. The products were blotted with anti-SMAC antibodies.

E3 regulation (37). To assess the effects of ubiquitin variants on AREL1 activity, we expressed and purified a previously published ubiquitin variant of AREL1 (UbV KL.3) (37), selected based on its maximum affinity (EC_{50} value) for AREL1. Based on our observation, KL.3 is a dimer in solution (Fig. S8). We incubated the extended AREL1 HECT domain with KL.3 in a 1:1 molar ratio and performed gel filtration using an S200 analytical column. We noted a shift in the profile of the extended AREL1 HECT:KL.3 sample, suggestive of a strong interaction (Fig. 7*A*). We next performed isothermal titration calorimetry (ITC) experiments to determine the binding affinities between the extended AREL1 HECT domain and UbV KL.3. The ITC experiments showed a dissociation coefficient of 427 nM for KL.3 binding to the extended AREL1 HECT domain (Fig. 7*B*). To confirm that KL.3 does not affect the functions of E1 (UBA1) and E2 (UbcH7) enzymes, we prepared a reaction mixture containing E1, E2, Ub, ATP, and KL.3 (10 and 20 μM) and kept the reaction at 37 °C for 1 h. SDS-PAGE analysis (nonreducing and reducing) of the reaction mixture showed that KL.3 does not inhibit the functions of E1 and E2 enzymes, as the formation of E2-Ub was unaffected in the presence of KL.3 (Fig. 7, *C* and *D*). We then performed an *in vitro* ubiquitination assay with 0.05 μM UBA1, 1 μM UbcH7, 3 μM extended AREL1 HECT, 20 μM WT Ub, and 10 μM SMAC. Two different concentrations (10 and 20 μM) of KL.3 were used in the ubiquitination assay. Interestingly, we observed that KL.3 hinders AREL1-mediated ubiquitination of SMAC, as noted by a decrease in the intensity of the ubiquitinated bands (Fig. 7, *E* and *F*). This suggests a possibility of modulating HECT E3 activity with ubiquitin variants.

The N-terminal extended region (aa 436–482) is critical for AREL1 stability and activity

The N-terminal extended region preceding the HECT domain has been shown to affect the stability and activity of HECT E3 ligases (30). A close examination of the structure of extended AREL1 HECT domain showed that the residues from the extended region are involved in the interactions with N-lobe residues (Fig. S3 and Table S2). Notably, Phe^{439} and Phe^{446} of the extended region form a hydrophobic cluster with the side chains of residues from the N-lobe. Furthermore, to explore the significance of the N-terminal extended region (aa 436–482) in AREL1 HECT stability and activity, we purified the AREL1 HECT domain alone (aa 483–823). We then performed a proteoplex assay to measure the melting temperatures (T_m) to assess protein stability (38, 39). Notably, we observed that the AREL1 HECT domain without the extended region shows temperature-dependent thermal denaturation at 37.6 ± 0.3 °C as compared with the extended AREL1 HECT domain (46.9 ± 0.17 °C) (Fig. 8*B*). This suggests that the extended N-terminal region is essential in providing the stability to the AREL1 HECT domain (Fig. S9). Furthermore, an *in vitro* ubiquitination assay of GST-tagged AREL1 HECT domain (aa 483–823) showed no catalytic activity for autoubiquitination. No higher-molecular weight bands corresponding to ubiquitinated AREL1 were observed in SDS-PAGE or Western blot analysis blotted with anti-ubiquitin antibodies for autoubiquitination, as compared with GST-tagged extended AREL1 HECT domain (aa 436–823) (Fig. 8, *C* and *D*). Similarly, for SMAC ubiquitination, SDS-PAGE and Western blot analysis blotted with anti-SMAC antibodies demonstrated that no SMAC ubiquitination was achieved with GST-tagged HECT domain alone (Fig. 8, *E* and *F*). This suggests that the deletion of this extended region completely hinders AREL1 catalytic activity, and this region is indispensable for the E3 ligase activity of AREL1. The CD spectra of the AREL1 HECT domain and the extended AREL1 HECT domain are similar (Fig. 8*A*).

Discussion

In the present study, we investigated AREL1, a member of the "other" subfamily of HECT E3 ligases. We solved the crystal structure of its extended HECT domain (aa 436–823) at 2.4 Å and showed that the N-lobe and C-lobe are folded into an inverted T-shaped conformation. The N-terminal extended region is critical for the activity and stability of AREL1 HECT domain. The deletion of this extended region substantially affected stability and rendered the AREL1 HECT domain inactive. Among the members of the "other" subfamily of HECT E3 ligases, only the crystal structures of E6AP and HUWE1 have been solved. The extended region (aa 3993–4012) preceding the HUWE1 HECT domain also confers stability; however, the HUWE1 HECT domain alone is capable of autoubiquitination and Mcl-1 substrate ubiquitination (30). Moreover, the authors showed that the addition of the extended region (aa 3993–4012) preceding the HUWE1 HECT domain decreased its autoubiquitination and substrate ubiquitination activities (30). Collectively, these studies point to the differential role of the extended region preceding the HECT domain on the stability and activity of the "other" subfamily of HECT E3 ligases.

AREL1 assembled Lys^{33}-, Lys^{48}-, and Lys^{63}-linked polyubiquitin chains during autoubiquitination. Lys^{48}- and Lys^{63}-linked chains are well-known markers for protein degradation and cellular signaling, respectively (8), which might allow AREL1 to regulate its activity in cells. However, the biological significance of Lys^{33}-linked chains is less understood (8). We further showed that the extended AREL1 HECT domain targets Lys^{62} and Lys^{191} residues on SMAC protein for ubiquitination and solved the crystal structure of the tetrameric form of SMAC, identifying the positions of these lysine residues. Moreover, we observed that the Glu^{701} residue makes multiple hydrogen-bonding contacts, and a E701A mutation substantially enhances AREL1 autopolyubiquitination and SMAC ubiquitination. Notably, a previous study found that mutation of an equivalent glutamic acid (E798V) in the HECT domain of WWP1 (NEDD4 subfamily) resulted in an increase in its autopolyubiquitination activity and subsequent constitutive expression in prostate cancer (40). Furthermore, mutation of a conserved phenylalanine to alanine (F820A), which is placed at the fourth position from the C terminus, and deletion of the last three amino acids at the C terminus (Δ3 CT) of AREL1 HECT domain completely blocks its autoubiquitination activity. The F820A mutants also displayed no SMAC ubiquitination, whereas the Δ3 CT mutants showed reduced SMAC ubiquitination. Previous studies have shown that phenylalanine placed at the fourth position from the C terminus is indispensable for isopeptide bond formation in the ubiquitination process (36). The authors proposed that this residue might be involved in the correct orien-

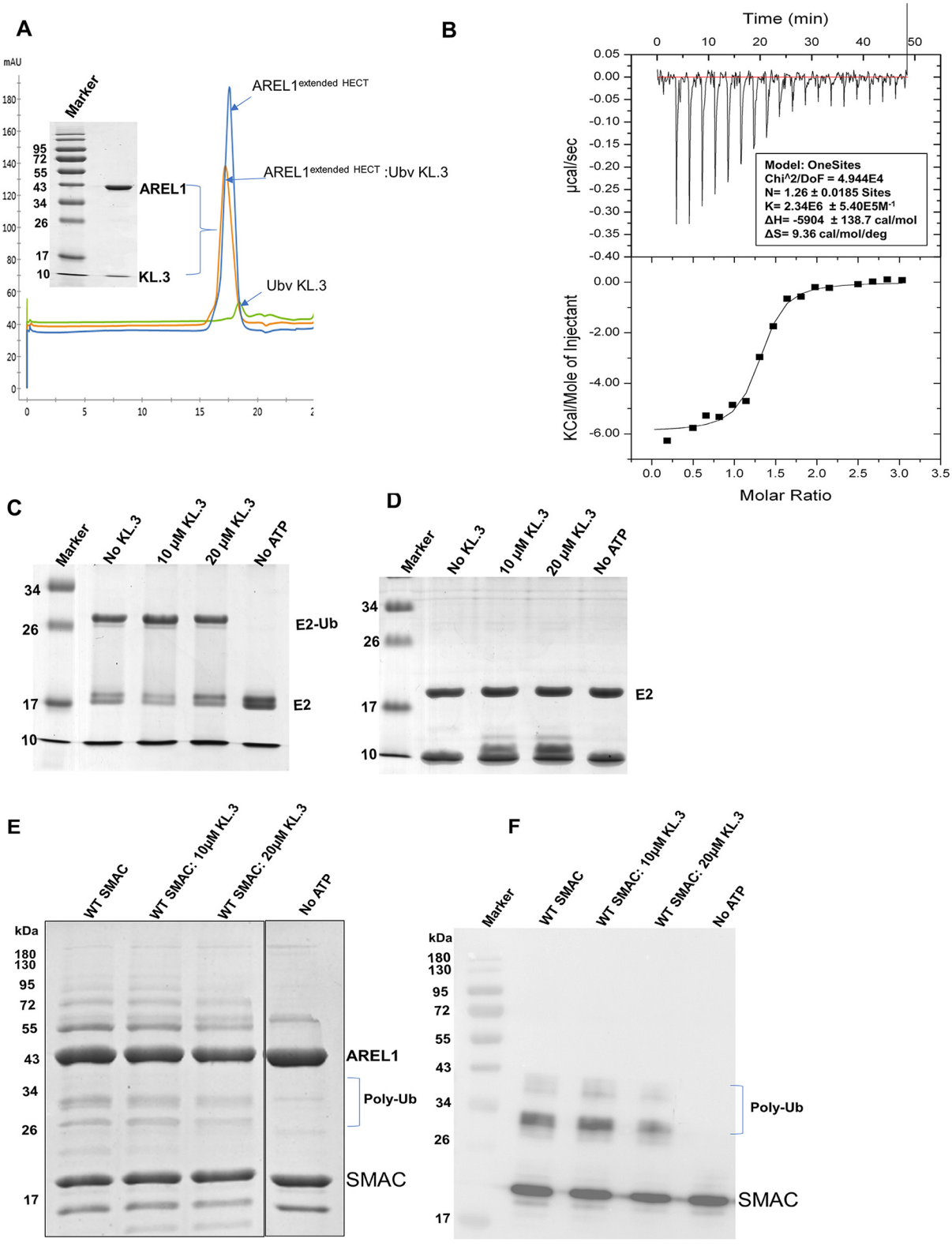

Figure 7. Extended AREL1 HECT interaction with ubiquitin variant KL.3. *A*, analytical S200 profiles of the extended AREL1 HECT domain (*blue*), KL.3 (*green*), and AREL1 HECT:KL.3 mixture (*orange*). SDS-PAGE image analysis of the extended AREL1 HECT:KL.3 mixture to show that both proteins interact and elute together. *B*, isothermal titration calorimetry profile to show the interaction between the extended AREL1 HECT domain and ubiquitin variant KL.3. Nonreducing SDS-PAGE (*C*) and reducing SDS-PAGE (*D*) analysis showed that KL.3 has no effects on the activities of E1 and E2 enzymes. *E*, SDS-PAGE analysis showing extended AREL1- mediated SMAC *in vitro* ubiquitination assay in the presence of ubiquitin variant KL.3. *F*, Western blot analysis of *E* to highlight extended AREL1-mediated SMAC ubiquitination in the presence of KL.3. The products were immunoblotted with anti-SMAC antibody.

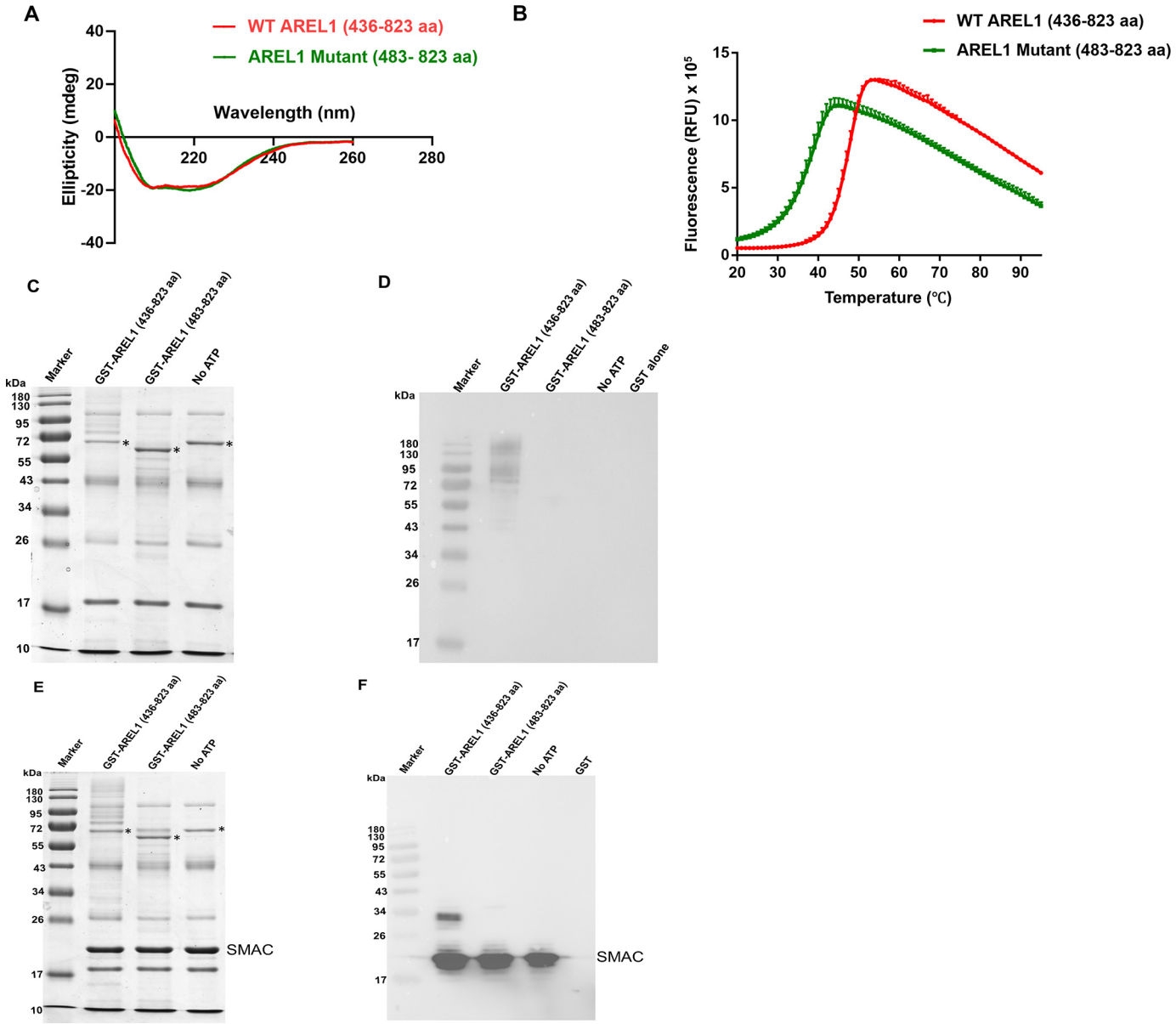

Figure 8. The N-terminal extended region is indispensable for AREL1 HECT domain stability and activity. *A*, the CD experiment showed structural similarities between the extended HECT and HECT domain alone of AREL1 E3 ligase. *B*, thermal denaturation curves for different AREL1 constructs. WT AREL1 (aa 436–823) (*red*), AREL1 mutant (aa 483–823) (*green*). A first derivative method was used to calculate the corresponding T_m values for these constructs. Each measurement was carried out in triplicate ± S.D. *RFU*, relative fluorescence units. SDS-PAGE analysis (*C*) and Western blot analysis (*D*) showed a complete loss of function of the AREL1 HECT domain (aa 483–823) as compared with the extended AREL1 HECT domain (aa 436–823). The products were blotted with anti-Ub antibodies. *, different constructs of the AREL1 HECT domain. *E* and *F*, SDS-PAGE analysis (*E*) and Western blot analysis (*F*) of AREL1 HECT domain alone on SMAC ubiquitination as compared with extended AREL1 HECT domain. *, different constructs of AREL1 HECT domain. The products were blotted with anti-SMAC antibodies.

tation of the ubiquitin molecule to form the isopeptide bond. The extended AREL1 HECT possesses an additional loop region in its N-lobe large subdomain, which is absent in all other HECT members. Deletion of this region slightly increased its autoubiquitination activity while not affecting AREL1-mediated SMAC ubiquitination (Fig. S10).

We next observed that the extended AREL1 HECT domain displayed weak ubiquitination activity in the absence of an E2 enzyme. Notably, members of the RBR E3 ligase family, such as Parkin and HOIP, were found to perform E2-independent ubiquitination (41, 42). However, a second report showed that Parkin depends on E2 enzyme for its activity (43), and therefore the physiological significance of E2-independent ubiquitination needs to be evaluated *in vivo*. For instance, FATS was identified as an E2-independent E3 ubiquitin ligase that can ubiquitinate and stabilize p53 in the absence of an E2 enzyme. However, FATS does not belong to any known E3 ligase family (44). Our observations led us to speculate that some HECT E3s might directly interact with the E1-Ub thioester to catalyze ubiquitin transfer to the catalytic cysteine, rendering the action of the E2 enzyme redundant. Nevertheless, our study shows that the efficiency of AREL1-mediated ubiquitination is significantly greater in the presence of the E2 enzyme.

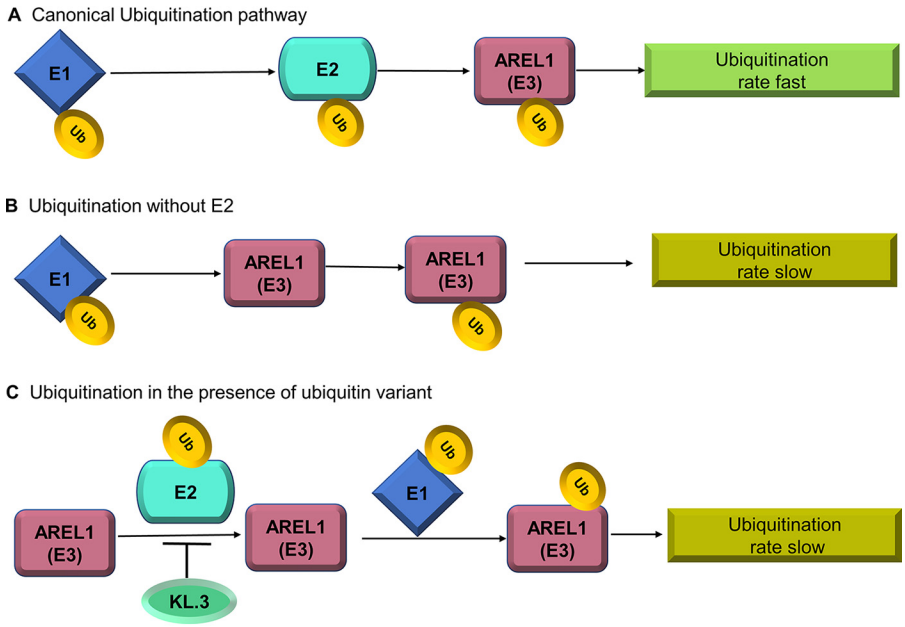

Figure 9. Proposed model for the extended AREL1 HECT ubiquitination. *A*, canonical ubiquitination pathway involves the enzymatic activities of E1 activating, E2 conjugating, and E3 ubiquitin ligase enzymes. *B*, the extended AREL1 HECT domain displays E2-independent autoubiquitination and substrate ubiquitination activity, via interacting directly with the E1 activating enzyme; however, this observed ubiquitination rate is lower than the canonical pathway. *C*, KL.3 might inhibit UbchH7 (E2)-AREL1 (E3) interaction in the canonical ubiquitination pathway, thus slowing down the ubiquitination process.

The recent structural and functional analysis of the NEDD4 subfamily of HECT E3s with engineered UbVs has paved the way for the design of therapeutic interventions that can modulate NEDD4 HECT E3 ligase activity (37). Here, we observed a strong interaction of the extended AREL1 HECT domain with its selective UbV KL.3, which reduced AREL1-mediated SMAC ubiquitination *in vitro*. Although the mechanism of action is still not clear, these engineered UbVs, with inhibitor-like potential, were shown to hijack the E2 binding site on NEDD4 HECT E3 members (37). This implies that KL.3 might function as an inhibitor UbV and could inhibit the AREL1-UbcH7 interaction, thereby slowing down the rate of ubiquitination (Fig. 9).

In summary, we have solved the crystal structure of an extended AREL1 HECT domain that forms an inverted T-shape conformation and harbors a unique loop region that is absent in other HECT members. We showed that the extended region preceding the AREL1 HECT domain is indispensable for its stability and activity. The extended AREL1 HECT domain is functionally active and assembles Lys^{33}-, Lys^{48}-, and Lys^{63}-linked polyubiquitin chains. Furthermore, we identified that Glu^{701} and the last three amino acids at the C terminus in the HECT domain are crucial for AREL1 activity. Due to the crucial role of SMAC in triggering apoptosis, several SMAC-mimetic compounds have been generated based on its dimeric crystal structure (45). However, the endogenously relevant tetrameric form of SMAC was not available earlier. Based on our study of AREL1-mediated SMAC ubiquitination, we were able to identify the possible ubiquitination sites (Lys^{62} and Lys^{191}) on SMAC, which we further mapped after solving the tetrameric structure of SMAC. Collectively, the structural and functional analysis of the extended AREL1 HECT domain–mediated SMAC ubiquitination could provide the platform for the therapeutic development of inhibitor molecules to target its activity in a broad range of cancers.

Materials and methods

Protein expression and purification

The protein constructs used in this study are listed in Table S1. The clones were confirmed through DNA sequencing, and all clones were expressed in *Escherichia coli BL21* (*DE3*). His_6-SUMO–tagged extended AREL1 HECT domain was purified by nickel-nitrilotriacetic acid affinity chromatography and desalted in Tris buffer (20 mM Tris, pH 8, 150 mM NaCl, 5% glycerol, 1 mM DTT), subsequently treated with SUMO protease for overnight cleavage at 4 °C, followed by gel filtration chromatography with HEPES buffer (20 mM HEPES, pH 8.0, 150 mM NaCl, 5% glycerol, 1 mM DTT). E1 (UBA1) was purified by nickel-nitrilotriacetic acid purification, whereas GST-tagged AREL1 constructs, ubiquitin, E2 (UbcH7), and UbV KL.3 were purified by GSH-affinity chromatography followed by gel filtration chromatography (Superdex S75 column). GST-tagged SMAC was purified with ion-exchange chromatography (HiTrap Q HP anion exchange) followed by gel filtration chromatography (Superdex S75 column) using the ÄKTA pure chromatography system (GE Healthcare). The GST tag was cleaved from the proteins using PreScission Protease (GE Healthcare) prior to gel filtration chromatography.

Reductive alkylation

Reductive alkylation was conducted with a commercially available reductive alkylation kit (Hampton Research) as described previously (46). Subsequently, gel filtration chromatography was performed in a buffer consisting of 10 mM Tris, pH 8.5, 150 mM NaCl, 5% glycerol, 1 mM DTT to separate the methylated protein sample.

Crystallization and structure determination of extended AREL1 HECT domain

The crystal screening of the extended AREL1 HECT domain was carried out using commercially available crystallization screens by incubating 1 μl of protein solution (10 mg/ml) with 1 μl of crystallization solution in a hanging-drop vapor-diffusion method. Crystals appeared after 3 days in 100 mM BisTris, pH 5.5, 200 mM ammonium sulfate at room temperature (23 °C) and were further optimized for obtaining diffraction quality crystals. The suitable crystals were immersed in mother liquor solution with 25% ethylene glycol as a cryoprotectant for synchrotron data collection. Complete native diffraction data were collected at 2.4 Å at the beamline MX2 Australian Synchrotron, part of ANSTO. Data were processed with the HKL-2000 program (47). The crystals belonged to space group C121 with three molecules in the asymmetric unit. CCP4 online program Balbes (48) generated an initial model with ITCH HECT (PDB code 3TUG) as the template (33% sequence identity), which was used in Phenix-Phaser for molecular replacement (49). The remaining model was built manually in COOT (50) and further refined using Phenix.Refine (49). The final model was refined at 2.4 Å resolution with an *R*-factor of 0.18 (R_{free} = 0.21) and has good stereochemical parameters evaluated with PROCHECK (51) (Table 1). PyMOL (52) was used to prepare all structure-related figures.

Crystallization and structure determination of SMAC

SMAC crystallization was carried out by incubating 1 μl of protein solution (4 mg/ml) with 1 μl of crystallization solution. The crystals were obtained with a condition consisting of 200 mM potassium phosphate monobasic, 20% PEG 3350, and complete native diffraction data were collected at 2.8 Å at the beamline 24-ID-E, APS, US. The structure was solved by molecular replacement in Phenix-Phaser using the monomeric form of SMAC protein (PDB code 1G73) as the search model. The remaining model was built manually in COOT and refined using Phenix.Refine. The current *R*-factor is 0.21 (R_{free} = 0.26) with good stereochemical parameters evaluated with PROCHECK (Table 1).

In vitro ubiquitination assays

Multiple *in vitro* ubiquitination assays were conducted to characterize the functional activity of the extended AREL1 HECT domain. The reaction mixtures contain 0.05 μM UBA1, 1 μM UbcH7, 3 μM WT extended AREL1 HECT or its mutants, 10 μM WT ubiquitin or its mutants, UbV KL.3 (10–20 μM), and 10 μM WT SMAC or its mutants. The ubiquitination mixtures were incubated at 37 °C for 120 min in 50 mM HEPES, pH 7.5, 100 mM NaCl, 5 mM ATP, 10 mM $MgCl_2$, 1 mM DTT. The ubiquitination reaction was terminated with the addition of SDS-PAGE loading buffer prior to 12.5% SDS-PAGE analysis.

Western blotting

SDS-polyacrylamide gels were transferred to polyvinylidene difluoride membranes (Sigma-Aldrich) followed by incubation with mouse monoclonal anti-SMAC antibody at 1:2000 dilutions or mouse monoclonal anti-ubiquitin antibody at 1:2000 dilutions (Santa Cruz Biotechnology, Inc.). After washing, membranes were incubated with horseradish peroxidase–conjugated secondary antibodies (Jackson ImmunoResearch) in a 1:10,000 dilution. The bands were visualized using ECL Western blotting substrate (Pierce) as instructed by the manufacturer. PageRuler Prestained protein ladder (catalogue no. 26616; lot 00355719; Thermo Scientific) was used in all of the gels to compare the protein bands.

Mass spectrometry

Following 12.5% SDS-PAGE analysis, bands corresponding to ubiquitinated species were excised and subjected to exhaustive trypsin digestion. Eksigent nanolC Ultra and ChiPLC-nanoflex (Eksigent, Dublin, CA) system was used in the Trap Elute configuration to separate peptides. The desalting of samples was performed with a Sep-Pak tC18 μElution Plate (Waters, Milford, MA) and subsequently reconstituted with 20 μl of diluent (98% water, 2% acetonitrile, 0.05% formic acid). The samples (2 μl) were loaded on a 200 μm × 0.5-mm trap column followed by elution on an analytical 75 μm × 150-mm column. Peptides were separated by a gradient formed by 2% acetonitrile, 0.1% formic acid (mobile phase A) and 98% acetonitrile, 0.1% formic acid (mobile phase B): 5–7% of mobile phase B in 0.1 min, 7–30% of mobile phase B in 10 min, 30–60% of mobile phase B in 4 min, 60–90% of mobile phase B in 5 min, 90 to 5% of mobile phase B in 0.1 min and 5 to 5% of mobile phase B in 10 min, at a flow rate of 300 nl/min. The TripleTOF 5600 system (AB SCIEX, Foster City, CA) was used to perform MS analysis in an information-dependent mode. MS spectra were acquired across the mass range of 400–1800 m/z in high-resolution mode (>30,000) using 250-ms accumulation time per spectrum. A maximum of 20 precursors per cycle were chosen for fragmentation from each MS spectrum with 100-ms minimum accumulation time for each precursor and dynamic exclusion for 15 s. Tandem mass spectra were recorded in high-sensitivity mode (resolution >15,000) with rolling collision energy on. Peptide identification and quantification were performed on the ProteinPilot™ 5.0 software Revision 4679 (AB SCIEX) using the Paragon™ database search algorithm (5.0.0.0, 4767) and the integrated false discovery rate analysis function. The data were searched against a database consisting of 2018_Juneuniprot_sprot (total 40,698 entries). The processing was specified as follows: digestion, trypsin; ID focus, biological modifications; special factors, ubiquitin/SUMO enrichment; search effort, thorough; detected protein threshold, 0.05 (10.0%). For false discovery rate determination, data were searched against a concatenated database with *in silico* on-the-fly reversal for decoy sequences automatically by the software. Peptides identified with confidence interval ≥95% were considered.

ITC

ITC experiments were performed using the MicroCal VP-ITC titration calorimeter (MicroCal, Northampton, MA). The extended AREL1 HECT domain and UbV KL.3 were purified separately in a buffer containing 20 mM Tris, pH 8.5, 100 mM NaCl, and 1 mM DTT. Both proteins were further concentrated to achieve a molar ratio of 1:10. All samples were spun and

degassed before the experiment. A single-ligand-binding site approach was employed to analyze binding isotherms as implemented in Origin 7 (OriginLab).

CD spectrometry

Far-UV spectra (260–200 nm) measurements of the extended AREL1 HECT domain and its mutants were performed using a Jasco J-100 spectropolarimeter (Jasco Europe, Cremella, Italy) in 20 mM Tris, 150 mM NaCl, and 2 mM DTT (pH 8) at room temperature (23 °C) using a 0.1-cm path length and stoppered cuvettes. Ten scans were recorded and averaged, and the baseline was subtracted.

Thermal stability analysis using proteoplex assay

The T_m measurements of different AREL1 constructs were performed in 96-well plates (Bio-Rad) using a quantitative PCR machine. The reaction mixture of 20 μl consisted of 18 μl of protein sample (1.0 mg/ml) in 20 mM Tris, pH 8, 150 mM NaCl, 5 mM DTT, and 2 μl of Sypro Orange (10×, Life Technologies, Inc.). The melting curves were measured by increasing the temperature from 10 to 95 °C at a ramp rate of 1% (1 °C/min). Raw temperature-dependent fluorescence signals were recorded based on thermal denaturation of AREL1 constructs. To process the data, the first derivative algorithm was used in a Microsoft Excel macro to calculate the temperature at which the upward slope of the fluorescence *versus* temperature curve is the steepest (T_m) (53). Each measurement was carried out in triplicate ± S.D.

Author contributions—S. S. and J. S. conceptualization; S. S. data curation; S. S. software; S. S., J. N., and J. S. formal analysis; J. S. supervision; S. S., D. N., and J. S. validation; S. S., J. N., and J. S. investigation; S. S., J. N., and J. S. visualization; S. S. and J. N. methodology; S. S. and J. S. writing-original draft; S. S. and J. S. writing-review and editing; J. S. resources; J. S. funding acquisition; J. S. project administration.

Acknowledgments—We acknowledge the beamline MX2 Australian Synchrotron, part of ANSTO, and NECAT beamline 24-ID-E at the Advanced Photon Source, Argonne National Laboratory. NECAT beamlines are funded by NIGMS, National Institutes of Health (NIH), Grant P41 GM103403. The Pilatus 6M detector on the 24-ID-E beamline is funded by NIH-ORIP HEI Grant S10 RR029205. The Advanced Photon Source is a United States Department of Energy User Facility operated by Argonne National Laboratory under Contract DE-AC02-06CH11357. We acknowledge the Protein and Proteomics center (NUS) for MS proteomics data acquisition and deposition.

References

1. Kwon, Y. T., and Ciechanover, A. (2017) The ubiquitin code in the ubiquitin-proteasome system and autophagy. *Trends Biochem. Sci.* **42,** 873–886 CrossRef Medline
2. Su, V., and Lau, A. F. (2012) Ubiquitination, intracellular trafficking, and degradation of connexins. *Arch. Biochem. Biophys.* **524,** 16–22 CrossRef Medline
3. Corn, J. E., and Vucic, D. (2014) Ubiquitin in inflammation: the right linkage makes all the difference. *Nat. Struct. Mol. Biol.* **21,** 297–300 CrossRef Medline
4. Fu, Y., Zhu, Y., Zhang, K., Yeung, M., Durocher, D., and Xiao, W. (2008) Rad6-Rad18 mediates a eukaryotic SOS response by ubiquitinating the 9-1-1 checkpoint clamp. *Cell* **133,** 601–611 CrossRef Medline
5. Pickart, C. M. (2001) Mechanisms underlying ubiquitination. *Annu. Rev. Biochem.* **70,** 503–533 CrossRef Medline
6. Wang, D., Ma, L., Wang, B., Liu, J., and Wei, W. (2017) E3 ubiquitin ligases in cancer and implications for therapies. *Cancer Metastasis Rev.* **36,** 683–702 CrossRef Medline
7. Scheffner, M., and Staub, O. (2007) HECT E3s and human disease. *BMC Biochem.* **8,** S6 CrossRef Medline
8. Kulathu, Y., and Komander, D. (2012) Atypical ubiquitylation: the unexplored world of polyubiquitin beyond Lys48 and Lys63 linkages. *Nat. Rev. Mol. Cell Biol.* **13,** 508–523 CrossRef Medline
9. Maspero, E., Mari, S., Valentini, E., Musacchio, A., Fish, A., Pasqualato, S., and Polo, S. (2011) Structure of the HECT:ubiquitin complex and its role in ubiquitin chain elongation. *EMBO Rep.* **12,** 342–349 CrossRef Medline
10. Maspero, E., Valentini, E., Mari, S., Cecatiello, V., Soffientini, P., Pasqualato, S., and Polo, S. (2013) Structure of a ubiquitin-loaded HECT ligase reveals the molecular basis for catalytic priming. *Nat. Struct. Mol. Biol.* **20,** 696–701 CrossRef Medline
11. Goka, E. T., and Lippman, M. E. (2015) Loss of the E3 ubiquitin ligase HACE1 results in enhanced Rac1 signaling contributing to breast cancer progression. *Oncogene* **34,** 5395–5405 CrossRef Medline
12. Besche, H. C., Sha, Z., Kukushkin, N. V., Peth, A., Hock, E.-M., Kim, W., Gygi, S., Gutierrez, J. A., Liao, H., Dick, L., and Goldberg, A. L. (2014) Autoubiquitination of the 26S proteasome on Rpn13 regulates breakdown of ubiquitin conjugates. *EMBO J.* **33,** 1159–1176 CrossRef Medline
13. Kim, J. B., Kim, S. Y., Kim, B. M., Lee, H., Kim, I., Yun, J., Jo, Y. Y., Oh, T., Jo, Y. Y., Chae, H. D., and Shin, D. Y. (2013) Identification of a novel anti-apoptotic E3 ubiquitin ligase that ubiquitinates antagonists of inhibitor of apoptosis proteins SMAC, HtrA2, and ARTS. *J. Biol. Chem.* **288,** 12014–12021 CrossRef Medline
14. Wei, Y., Fan, T., and Yu, M. (2008) Inhibitor of apoptosis proteins and apoptosis. *Acta Biochim. Biophys. Sin.* (*Shanghai*) **40,** 278–288 CrossRef Medline
15. Mannhold, R., Fulda, S., and Carosati, E. (2010) IAP antagonists: promising candidates for cancer therapy. *Drug Discov. Today* **15,** 210–219 CrossRef Medline
16. Varfolomeev, E., Blankenship, J. W., Wayson, S. M., Fedorova, A. V., Kayagaki, N., Garg, P., Zobel, K., Dynek, J. N., Elliott, L. O., Wallweber, H. J. A., Flygare, J. A., Fairbrother, W. J., Deshayes, K., Dixit, V. M., and Vucic, D. (2007) IAP antagonists induce autoubiquitination of c-IAPs, NF-κB activation, and TNFα-dependent apoptosis. *Cell* **131,** 669–681 CrossRef Medline
17. Kristariyanto, Y. A., Choi, S., Arif, S., Rehman, A., Ritorto, M. S., Campbell, D. G., and Nicholas, A. (2015) Assembly and structure of Lys33-linked polyubiquitin reveals distinct conformations. *Biochem. J.* **467,** 345–352
18. Michel, M. A., Elliott, P. R., Swatek, K. N., Simicek, M., Pruneda, J. N., Wagstaff, J. L., Freund, S. M. V., and Komander, D. (2015) Assembly and specific recognition of K29- and K33-linked polyubiquitin. *Mol. Cell.* **58,** 95–109 CrossRef Medline
19. Ng, C., Jackson, R. A., Buschdorf, J. P., Sun, Q., Guy, G. R., and Sivaraman, J. (2008) Structural basis for a novel intrapeptidyl H-bond and reverse binding of c-Cbl-TKB domain substrates. *EMBO J.* **27,** 804–816 CrossRef Medline
20. Mukherjee, M., Chow, S. Y., Yusoff, P., Seetharaman, J., Ng, C., Sinniah, S., Koh, X. W., Asgar, N. F. M., Li, D., Yim, D., Jackson, R. A., Yew, J., Qian, J., Iyu, A., Lim, Y. P., Zhou, X., Sze, S. K., Guy, G. R., and Sivaraman, J. (2012) Structure of a novel phosphotyrosine-binding domain in Hakai that targets E-cadherin. *EMBO J.* **31,** 1308–1319 CrossRef Medline
21. Mukherjee, M., Jing-Song, F., Ramachandran, S., Guy, G. R., and Sivaraman, J. (2014) Dimeric switch of Hakai-truncated monomers during substrate recognition: insights from solution studies and NMR structure. *J. Biol. Chem.* **289,** 25611–25623 CrossRef Medline
22. Nayak, D., and Sivaraman, J. (2015) Structural basis for the indispensable role of a unique zinc finger motif in LNX2 ubiquitination. *Oncotarget* **6,** 34342–34357 CrossRef Medline

23. Nayak, D., and Sivaraman, J. (2018) Structure of LNX1:Ubc13∼ubiquitin complex reveals the role of additional motifs for the E3 ligase activity of LNX1. *J. Mol. Biol.* **430,** 1173–1188 CrossRef Medline
24. Tan, K., Kim, Y., Hatzos-Skintges, C., Chang, C., Cuff, M., Chhor, G., Osipiuk, J., Michalska, K., Nocek, B., An, H., Babnigg, G., Bigelow, L., Joachimiak, G., Li, H., Mack, J., *et al.* (2014) Salvage of failed protein targets by reductive alkylation. *Methods Mol. Biol.* **1140,** 189–200 CrossRef Medline
25. Sluimer, J., and Distel, B. (2018) Regulating the human HECT E3 ligases. *Cell. Mol. Life Sci.* **75,** 3121–3141 CrossRef Medline
26. Gong, W., Zhang, X., Zhang, W., Li, J., and Li, Z. (2015) Structure of the HECT domain of human WWP2. *Acta Crystallogr. F Struct. Biol. Commun.* **71,** 1251–1257 CrossRef Medline
27. Holm, L., and Laakso, L. M. (2016) Dali server update. *Nucleic Acids Res.* **44,** W351–W355 CrossRef Medline
28. Kamadurai, H. B., Souphron, J., Scott, D. C., Duda, D. M., Miller, D. J., Stringer, D., Piper, R. C., and Schulman, B. A. (2009) Insights into ubiquitin transfer cascades from a structure of a UbcH5B∼Ubiquitin-HECTNEDD4L complex. *Mol. Cell* **36,** 1095–1102 CrossRef Medline
29. Verdecia, M. A., Joazeiro, C. A. P., Wells, N. J., Ferrer, J. L., Bowman, M. E., Hunter, T., and Noel, J. P. (2003) Conformational flexibility underlies ubiquitin ligation mediated by the WWP1 HECT domain E3 ligase. *Mol. Cell.* **11,** 249–259 CrossRef Medline
30. Pandya, R. K., Partridge, J. R., Love, K. R., Schwartz, T. U., and Ploegh, H. L. (2010) A structural element within the HUWE1 HECT domain modulates self-ubiquitination and substrate ubiquitination activities. *J. Biol. Chem.* **285,** 5664–5673 CrossRef Medline
31. Huang, L., Kinnucan, E., Wang, G., Beaudenon, S., Howley, P. M., Huibregtse, J. M., and Pavletich, N. P. (1999) Structure of an E6AP-UbcH7 complex: insights into ubiquitination by the E2-E3 enzyme cascade. *Science* **286,** 1321–1326 CrossRef Medline
32. Chai, J., Du, C., Wu, J. W., Kyin, S., Wang, X., and Shi, Y. (2000) Structural and biochemical basis of apoptotic activation by Smac/DIABLO. *Nature* **406,** 855–862 CrossRef Medline
33. Mastrangelo, E., Vachette, P., Cossu, F., Malvezzi, F., Bolognesi, M., and Milani, M. (2015) The activator of apoptosis Smac-DIABLO acts as a tetramer in solution. *Biophys. J.* **108,** 714–723 CrossRef Medline
34. Krissinel, E., and Henrick, K. (2007) Inference of macromolecular assemblies from crystalline state. *J. Mol. Biol.* **372,** 774–797 CrossRef Medline
35. Kim, H. C., and Huibregtse, J. M. (2009) Polyubiquitination by HECT E3s and the determinants of chain type specificity. *Mol. Cell. Biol.* **29,** 3307–3318 CrossRef Medline
36. Salvat, C., Wang, G., Dastur, A., Lyon, N., and Huibregtse, J. M. (2004) The −4 phenylalanine is required for substrate ubiquitination catalyzed by HECT ubiquitin ligases. *J. Biol. Chem.* **279,** 18935–18943 CrossRef Medline
37. Zhang, W., Wu, K.-P., Sartori, M. A., Kamadurai, H. B., Ordureau, A., Jiang, C., Mercredi, P. Y., Murchie, R., Hu, J., Persaud, A., Mukherjee, M., Li, N., Doye, A., Walker, J. R., Sheng, Y., *et al.* (2016) System-wide modulation of HECT E3 ligases with selective ubiquitin variant probes. *Mol. Cell.* **62,** 121–136 CrossRef Medline
38. Prinz, F., Puetter, V., Holton, S. J., Andres, D., Stegmann, C. M., Kwiatkowski, D., Prechtl, S., Petersen, K., Beckmann, G., Kreft, B., Mumberg, D., and Fernández-Montalván, A. (2016) Functional and structural characterization of Bub3·BubR1 interactions required for spindle assembly checkpoint signaling in human cells. *J. Biol. Chem.* **291,** 11252–11267 CrossRef Medline
39. Kozak, S., Lercher, L., Karanth, M. N., Meijers, R., Carlomagno, T., and Boivin, S. (2016) Optimization of protein samples for NMR using thermal shift assays. *J. Biomol. NMR* **64,** 281–289 CrossRef Medline
40. Courivaud, T., Ferrand, N., Elkhattouti, A., Kumar, S., Levy, L., Ferrigno, O., Atfi, A., and Prunier, C. (2015) Functional characterization of a WWP1/Tiul1 tumor-derived mutant reveals a paradigm of its constitutive activation in human cancer. *J. Biol. Chem.* **290,** 21007–21018 CrossRef Medline
41. Chew, K. C. M., Matsuda, N., Saisho, K., Lim, G. G. Y., Chai, C., Tan, H. M., Tanaka, K., and Lim, K. L. (2011) Parkin mediates apparent E2-independent monoubiquitination *in vitro* and contains an intrinsic activity that catalyzes polyubiquitination. *PLoS One* **6,** e19720 CrossRef Medline
42. Smit, J. J., Monteferrario, D., Noordermeer, S. M., van Dijk, W. J., van der Reijden, B. A., and Sixma, T. K. (2012) The E3 ligase HOIP specifies linear ubiquitin chain assembly through its RING-IBR-RING domain and the unique LDD extension. *EMBO J.* **31,** 3833–3844 CrossRef Medline
43. Trempe, J., Sauvé, V., Grenier, K., Seirafi, M., Tang, M. Y., Ménade, M., Al-Abdul-Wahid, S., Krett, J., Wong, K., Kozlov, G., Nagar, B., Fon, E. A., and Gehring, K. (2013) Structure of Parkin reveals mechanisms for ubiquitin ligase. *Science* **340,** 1451–1455 CrossRef Medline
44. Yan, S., Qiu, L., Ma, K., Zhang, X., Zhao, Y., Zhang, J., Li, X., Hao, X., and Li, Z. (2014) FATS is an E2-independent ubiquitin ligase that stabilizes p53 and promotes its activation in response to DNA damage. *Oncogene* **33,** 5424–5433 CrossRef Medline
45. Fulda, S., and Vucic, D. (2012) Targeting IAP proteins for therapeutic intervention in cancer. *Nat. Rev. Drug Discov.* **11,** 109–124 CrossRef Medline
46. Shaw, N., Cheng, C., and Liu, Z.-J. (2007) Procedure for reductive methylation of protein to improve crystallizability. *Protoc. Exch.* 10.1038/nprot.2007.287 CrossRef
47. Otwinowski, Z., and Minor, W. (1997) Processing of X-ray diffraction data collected in oscillation mode. *Methods Enzymol.* **276,** 307–326 CrossRef Medline
48. Long, F., Vagin, A. A., Young, P., and Murshudov, G. N. (2008) BALBES: a molecular-replacement pipeline. *Acta Crystallogr. D Biol. Crystallogr.* **64,** 125–132 CrossRef Medline
49. Adams, P. D., Afonine, P. V., Bunkóczi, G., Chen, V. B., Davis, I. W., Echols, N., Headd, J. J., Hung, L.-W., Kapral, G. J., Grosse-Kunstleve, R. W., McCoy, A. J., Moriarty, N. W., Oeffner, R., Read, R. J., Richardson, D. C., *et al.* (2010) PHENIX: a comprehensive Python-based system for macromolecular structure solution. *Acta Crystallogr. D Biol. Crystallogr.* **66,** 213–221 CrossRef Medline
50. Emsley, P., and Cowtan, K. (2004) Coot: model-building tools for molecular graphics. *Acta Crystallogr. D Biol. Crystallogr.* **60,** 2126–2132 CrossRef Medline
51. Laskowski, R. A., MacArthur, M. W., and Moss, D. S. T. J. (1993) Procheck: a program to check the stereochemical quality of protein structures. *J. Appl. Crystallogr.* **26,** 283–291 CrossRef
52. DeLano, W. L. (2012) *The PyMOL Molecular Graphics System*, version 1.5.0.1, Schroedinger, LLC, New York
53. Chari, A., Haselbach, D., Kirves, J.-M., Ohmer, J., Paknia, E., Fischer, N., Ganichkin, O., Möller, V., Frye, J. J., Petzold, G., Jarvis, M., Tietzel, M., Grimm, C., Peters, J.-M., Schulman, B. A., *et al.* (2015) ProteoPlex: stability optimization of macromolecular complexes by sparse-matrix screening of chemical space. *Nat. Methods* **12,** 859–865 CrossRef Medline